Title

Cellular and cytoskeletal alterations of scleral fibroblasts in response to glucocorticoid steroids.

Authors

Bogarin, Thania
Saraswathy, Sindhu
Akiyama, Goichi
et al.

Publication Date

2019-10-01

DOI

10.1016/j.exer.2019.107774

Peer reviewed

HHS Public Access

Author manuscript

Exp Eye Res. Author manuscript; available in PMC 2020 October 01.

Published in final edited form as:

Exp Eye Res. 2019 October ; 187: 107774. doi:10.1016/j.exer.2019.107774.

Cellular and Cytoskeletal Alterations of Scleral Fibroblasts in Response to Glucocorticoid Steroids

Thania Bogarin[a], **Sindhu Saraswathy**[a], **Goichi Akiyama**[a], **Xiaobin Xie**[a,b], **Robert N. Weinreb**[c], **Jie Zheng**[d], **Alex S. Huang**[a]

[a]Doheny Eye Institute and Department of Ophthalmology, David Geffen School of Medicine at UCLA, Los Angeles, CA, USA

[b]Eye Hospital of China Academy of Chinese Medical Sciences, Beijing, China

[c]Hamilton Glaucoma Center, Shiley Eye Institute, and the Viterbi Family Department of Ophthalmology University of California, San Diego, CA, USA

[d]Stein Eye Institute and Department of Ophthalmology, David Geffen School of Medicine at UCLA, Los Angeles, CA, USA

Abstract

Steroid-induced ocular hypertension can be seen even after trabecular meshwork (TM) bypass/ablation. Thus, the purpose was to investigate steroid-response in cells distal to the TM by using primary scleral fibroblasts. Primary scleral cell cultures were generated using mid-depth scleral wedges from human donor corneo-scleral rims (n=5) after corneal transplantation. Cells were treated with dexamethasone (DEX; 100 nM) and compared to media (MED)/vehicle (DMSO) controls. Cell size, shape, and migration were studied using the IncuCyte Live-Cell Analysis System. Cytoskeleton was compared using Alexa Fluor-568 Phalloidin and senescence tested by evaluating beta-galactosidase. Western blot comparison was performed for α-SMA, FKBP-51, fibronectin, phospho-myosin light chain, and myocilin. Scleral fibroblasts upregulated FKBP-51 in response to DEX indicating the existence of steroid-responsive pathways. Compared to controls, DEX-treated cells proliferated slower (~50%; $p < 0.01–0.02$), grew larger (~1.3-fold; $p < 0.001$), and migrated less ($p = 0.01–0.006$). Alexa Fluor 568 Phalloidin actin stress fiber labeling was more diffuse in DEX-treated cells ($p = 0.001–0.004$). DEX-treated cells showed more senescence compared to controls (~1.7-fold; $p = 0.01–0.02$). However, DEX-treated cells did not show increased cross-linked actin network formation or elevated myocilin/fibronectin/α-SMA/phospho-myosin light chain protein expression. For all parameters, MED- and DMSO-treated control cells were not significantly different. Primary scleral fibroblasts, grown from tissue collected immediately distal to the TM, demonstrated scleral-response behaviors that were similar to, but not identical with, classic TM steroid-response. Further study is needed to understand how these

Corresponding Author: Alex Huang, MD/PhD, Doheny Eye Institute, Department of Ophthalmology, David Geffen School of Medicine, University of California, Los Angeles, 1355 San Pablo Street, Los Angeles, CA 90033, Ahuang@Doheny.org, Phone: 323-342-6436; Fax: 323-342-6688.

scleral cellular alterations may contribute to steroid-response IOP elevation after TM bypass/ablation surgery.

1. Introduction

Trabecular meshwork-targeted minimally invasive glaucoma surgeries (MIGS) safely lower intraocular pressure (IOP) in open-angle glaucomas (Chou et al., 2017). Typically conducted concurrent with cataract surgery, these procedures are performed by bypassing or ablating the trabecular meshwork (TM). The TM and Schlemm's canal (SC) border is where the majority of aqueous humor outflow (AHO) resistance resides (Johnson, 2006) so by creating a direct communication between the anterior chamber to SC, lower IOP can be achieved. However, the challenge for MIGS has been inconsistent frequency and magnitude of IOP reduction. Hypotheses for these results include unfavorable MIGS surgical placement in the setting of segmental (peri-limbal and non-circumferential) aqueous humor outflow (AHO) (Huang et al., 2018a; Huang et al., 2016a; Saraswathy et al., 2016; Vranka and Acott, 2017; Vranka et al., 2015; Xie et al., 2019), surgeon error, or steroid-response.

Steroid-response is defined by IOP elevation (ocular hypertension) after steroid exposure. It has been extensively studied after topical or systemic delivery with or without surgery. Steroid-response IOP elevation was first described in the 1950's after adrenocorticotropin hormone (ACTH) exposure (Gordon et al., 1951). While steroid-response can occur with systemic administration, topical steroid exposure on the eye has been particularly implicated with IOP elevation seen in ~30% of patients using an IOP endpoint of 20–31 mm Hg (Becker, 1965; Phulke et al., 2017) and in ~30% of patients when using an endpoint of 6–15 mm Hg elevation (Armaly, 1965; Phulke et al., 2017). The prevalence of steroid- induced ocular hypertension is even higher in patients with primary open angle glaucoma (Phulke et al., 2017; Weinreb et al., 1985). Mechanistically, steroid-response has been thoroughly studied at the TM. Using TM cell culture, steroid exposure led to larger cells (Clark et al., 1994; Clark and Wordinger, 2009; Tripathi et al., 1989; Wilson et al., 1993) that showed diminished proliferation (Clark and Wordinger, 2009; Wilson et al., 1993), phagocytosis (Bill, 1975; Clark and Wordinger, 2009; Matsumoto and Johnson, 1997), and migration (Clark et al., 1994; Clark and Wordinger, 2009). At a sub-cellular level, steroid exposure led to an increase in myocilin and fibronectin (Clark and Wordinger, 2009; Polansky et al., 1997; Polansky et al., 2000) protein expression as well as formation of cross-linked actin networks (CLANs) (Clark et al., 2005; Clark et al., 1996; Clark et al., 1994; Clark and Wordinger, 2009; Wilson et al., 1993). Upregulation of integrin avp3 via the calcineurin/NFAT pathway has been hypothesized to mediate some of these changes (Faralli et al., 2013).

After all intraocular surgeries, steroids are near universally used in order to control inflammation and its sequelae. Not unexpectedly, in some patients, post-operative steroids can also lead to steroid-induced ocular hypertension (Armaly, 1963; Becker, 1965; Becker and Mills, 1963). In several reports, a persistence of steroid-induced ocular hypertension has been observed, even after TM- targeted MIGS which circumvent the TM (Belovay et al., 2012; Fellman, 2015; Harvey and Khaimi, 2011; Karmel, 2014; Le and Saheb, 2014; Liu et

al., 2009). Thus, it has been recommended that topical steroids should be more rapidly tapered following MIGS procedures (Harvey and Khaimi, 2011; Le and Saheb, 2014).

For TM-targeted MIGS, the conundrum has been that steroid-induced ocular hypertension can persist despite TM bypass or ablation that creates a direct communication between the anterior chamber and SC. This is unexpected because if steroid-response is due to TM alterations, the question arises as to why and how it can persist if the TM is ablated or bypassed. This implies the possibility of a TM-independent steroid-response, and this phenomenon has been poorly characterized at an epidemiological, cellular and molecular level. Two hypotheses could help explain this seeming contradiction. First, in the setting of segmental AHO, if TM-targeted MIGS were placed at nonimprovable outflow regions, steroid-response could arise in the remaining AHO pathways (Huang et al., 2017b; Huang et al., 2017c; Huang et al., 2019; Huang et al., 2018b; Huang et al., 2016b; Huang et al., 2016c). Alternatively, there could be steroid-mediated changes in the distal outflow pathways past the TM (Huang et al., 2017a) (after SC, collector channels [CC's], intrascleral venous plexus, and aqueous/episcleral veins).

In this report, we study steroid-response distal to the TM. Ideally, cells lining the distal AHO pathways should be isolated for study, but there are no validated methods to purify and expand just these cells. Alternatively, we created scleral fibroblast cell culture, incubated the cells with steroids, and looked for steroid-mediated changes. We study some of the previously reported TM steroid-response endpoints (proliferation, cell size, cellular migration, myocilin, fibronectin, and cytoskeleton) in addition to other cellular characteristics. The scleral cells were derived from mid-depth scleral tissue taken from donor corneal transplant rims immediately posterior to TM and SC. This is important as this is where the distal outflow pathways are located. Moreover, this avoided the superficial episclera near Tenon's capsule and deeper lamina fusca sclera where there is retinal pigment epithelium and choroid. We hypothesize that scleral cells share some of the steroid-response characteristics with TM cells that may contribute to steroid-response in the distal AHO pathways and IOP elevation after TM-targeted MIGS.

2. Methods

2.1. Cell Culture

Scleral primary cultures were generated using previously published methods (Acott et al., 1988; Hernandez et al., 1987; Jobling et al., 2004; Tripathi and Tripathi, 1982). Briefly, corneal-scleral rims from 5 human donors were acquired after corneal transplantation surgeries under a UCLA approved IRB protocol. No subject had a known history of glaucoma or eye disease. Multiple mid-depth scleral wedges were dissected with careful attention to avoid manipulation of surface Tenon for concern of contamination (Fig. 1A). Explants were incubated in media (DMEM/F12; ThermoFisher Scientific, Waltham, MA) with 10% fetal bovine serum (VWR, Radnor, PA), and 1% antibiotics and antimycotics (penicillin, streptomycin, and amphotericin B; Corning, Corning, NY) at 37°C in 5% CO_2. Half of the media was replaced with fresh media every other day, and over several weeks spindle-shaped scleral fibroblasts migrated from the wedge onto the tissue culture plate. Scleral cells were passaged by treating confluent cells with trypsin (GenClone, El Cajon,

CA) at 37°C in 5% CO_2 for 5–10 minutes followed by media neutralization. All experiments were done on passage numbers 3–6.

2.2 Primary Scleral Cell Characterization

In general, scleral cells were seeded and grown to 70% confluence in 4-well chamber slides (ThermoFisher) under 3 treatment groups and treated daily for 7 days: DEX (100 nM dexamethasone dissolved in DMSO [Millipore Sigma, Burlington, MA]), DMSO (0.1% [Millipore Sigma]), and MED (media). After 7 days, cells were washed with 1X phosphate buffered saline (PBS; Millipore Sigma), fixed with 4% paraformaldehyde for 25 minutes at room temperature (RT), washed 3 times with PBS, and blocked/permeablized with 0.25% Triton X-100 in 5% bovine serum albumin (BSA; Rockland, Limerick, PA) for 30 minutes at RT. Fixed cells were incubated in α-smooth muscle actin primary antibody (α-SMA; ab5694; Abcam, Cambridge, MA; 1:100) with 1% BSA overnight at 4°C. Cells were then washed twice with PBS, incubated in Texas Red-X secondary antibody (T-6391; ThermoFisher) with 0.2% BSA for 1 hour at RT, stained/mounted with DAPI (Vector Laboratories, Burlingame, CA), and imaged under a BZ-X700 digital imaging microscope (Keyence, Itasca, IL).

2.2.1 Cell Proliferation—Scleral cells were seeded and grown in 96-well plates at a cell concentration of ~500 cells per well under the same 3 treatment groups (20 wells per group) and treated daily for 7 days. Cell images were taken with IncuCyte Live-Cell Analysis System (Essen BioScience, Ann Arbor, MI) and percent confluence determined by built-in software. To further confirm the automated cell counting, manual counting was also performed based on a sampling of original IncuCyte images. At 0, 10, 60, 80, 125, and 162 hour time points, cells were manually counted by masked graders (n = 3 images per condition). Three separate cell lines from two different donors were evaluated for both proliferation assessment methods. All data are expressed as a mean +/− SEM.

2.2.2 Cell Size Analyses—IncuCyte images were exported from the proliferation assay to ImageJ for cell size analyses using ImageJ software (Schneider et al., 2012) and quantitatively analyzed. Blinded graders used the ImageJ freehand tracing tool to trace individual cells and measure area. To standardize analyses, images were chosen based on the same cell confluence (~10%) for all 3 treatments in order to measure clear single cells. This meant evaluating DEX-treated cells at 72-hours and MED- and DMSO-treated cells at 48-hours. For each treatment condition, approximately 10 cells were measured, each from a total of 7 different wells for a total of 60 cells measured. Cells from three separate cell lines from two different donors were assessed.

2.3. Cytoskeletal labeling

Scleral cells were grown to 70% confluence in 4-well chamber slides (ThermoFisher) under the same treatment groups (4 wells per group). After 7 days, cells were fixed with 4% paraformaldehyde for 15 minutes at room temperature (RT) and blocked/permeablized with 0.25% Triton X-100 in 5% BSA for 30 minutes at RT. Fixed cells were incubated in phalloidin (Alexa Fluor 568 Phalloidin; ThermoFisher; 1:50) with 1% BSA overnight at 4°C, washed, stained/mounted with DAPI (Vector Laboratories), and viewed under a BZ-

X700 digital imaging microscope (Keyence). Cells form two separate cell lines from two different donors were assessed.

2.3.1 Quantitative Cytoskeletal Fluorescent Analysis—The above cytoskeletal fluorescence of filamentous actin stress fiber distribution was analyzed by using a bin-based pixel intensity approach. Phalloidin-stained images were converted to an 8-bit (black and white) format and uploaded to ImageJ software for analysis. Individual cells were traced with freehand tracing tool. The histogram command was selected to reveal the pixel intensity (0–255) distribution values for each of the selected cell images. Four bins were established based on pixel intensity (bin 1: pixel values 0–63, bin 2: 64–127, bin 3: 128–191, and bin 4: 192–255) to represent the ranges of signal intensities. In other words, bin 1 represented a collection of the darkest pixels, and bin 4 represented a collection of the brightest pixels. For each cell, the number of pixels within each bin was determined. For each treatment condition, 7–9 cells were measured from a total of 8 different wells for a total of 62 cells measured per condition with the average number of pixels per bin determined.

2.3.2 Cross-linked Actin Network Analyses—The above phalloidin-stained images were also examined for CLANs based on published criteria (Filla et al., 2009) and quantified. For each image, cells were analyzed and recorded as either a CLAN-positive cell (CPC) (Filla et al., 2011) or not (non-CPC). Images were taken from 4 individual wells per treatment. For each well, the total number of CPCs was divided by the total number of analyzed cells to yield the CPC percentage. The calculated values for each well were averaged across the 4 wells per treatment and converted to a final percentage.

2.4. Western Blotting

For protein expression experiments, whole cell-lysates were prepared using 1X RIPA lysis buffer (Millipore Sigma) with protease inhibitors (Millipore Sigma; 1:100) by shearing cells with a 22-gauge needle while kept on ice. Phosphatase inhibitors (Cocktail 2 at 1:100 and Cocktail 3 at 1:50; Millipore Sigma) were added for experiments looking at phosphorylation. Samples were centrifuged at 14,000 rpm for 25 minutes at 4°C two sequential times. The supernatant was then transferred to a chilled tube and protein concentration measured. For Western blot, samples were denatured and reduced with 2-mercaptoethanol (Bio-Rad, Hercules, CA) and Laemmli buffer (Bio-Rad) by boiling for 5 minutes followed by cooling on ice. Protein samples were loaded and separated on a 4–20% Mini-Protean TGX polyacrylamide gel (Bio-Rad) at RT followed by transfer onto a polyvinylidene difluoride (Bio-Rad) membrane at 4°C. The membrane was blocked with 5% blotting grade non-fat dry milk (Bio-Rad) or 5% BSA (Rockland) and 1x-Tris buffered saline (Bio-Rad) with Tween 20 (0.1%; Bio-Rad) for 1 hour RT or overnight at 4°C. Membranes were probed with antibodies to α-SMA (ab5694; Abcam; 1:500), FKBP-51 (ab79844; Abcam; 1:1000), myocilin (ab41552; Abcam; 1:500), fibronectin (ab2413; Abcam; 1:5000), myosin light chain 2 (3672; Cell Signaling, Danvers, MA; 1:1000), phospho-myosin light chain 2 (3674; Cell Signaling; 1:1000), or glyceraldehyde-3-phosphate dehydrogenase (GAPDH; MAB374; Millipore, Burlington, MA; 1:5000). Goat Anti-Rabbit IgG-HRP and Horse Anti-Mouse IgG-HRP (Vector Laboratories; 1:2000) were

used as secondary antibodies. Protein bands were imaged with a ChemiDoc XRS+ imaging system (BioRad). Quantitative band densitometry was performed using ImageJ.

2.5. Cellular Migration Assay

To test cellular migration, we created a wound in the cell culture into which cells could migrate and re-populate the region. Two scleral cell lines from two different donors were seeded and grown on 96-well plates at a cell concentration of ~1000 cells per well under the same 3 treatment groups (4 wells per group), and treated daily for 7 days with DEX, MED, or DMSO. At the end of day 7, wells were scratched with WoundMaker™ and washed. Drug treatment continued for 2.5 more days (~60-hours). Images were taken with IncuCyte Live-Cell Analysis System (Essen BioScience), and wound width, relative wound density, and wound confluence were determined by built-in software. Wound width was determined by taking the average distance between the edges of the initial scratch. In this measurement, isolated cells, not contiguous to the native (unscratched) cell population on each side of the wound were excluded per built-in software. Relative wound density was measured as the ratio of cell-density in the wound to the cell density in the native (unscratched) regions. Wound confluence percentage was the fractional wound area that was covered by cells.

2.5. Senescence Assay

To test for cellular senescence, scleral cells were seeded and grown on a 12-well plate at a cell concentration of ~2500 cells per well under the same 3 treatment groups (3 wells per group), and treated daily for 7 days with DEX, MED, or DMSO. At the end of day 7, cells were washed once with PBS and a fixative solution from a senescence detection kit (ab65351; Abcam) was applied for 25 minutes at RT. Cells were washed twice with PBS, treated with X-gal staining solution, inserted into a plastic bag, and placed in an incubator (37°C; 5% CO_2) overnight. Images were taken with a BZ-X700 digital imaging microscope (Keyence) at a 10X magnification. For each well, images with individual cells were counted and identified as either normal (not blue) or senescent (blue) by a masked grader. The number of blue cells was then divided by the total number of counted cells yielding the percentage of senescent cells within the image. The calculated values for each image was averaged across the 3 wells per treatment and converted into a final percentage.

3. Results

To study steroid-response distal to the TM, we created scleral fibroblast primary culture using mid-depth scleral wedges from remnant donor corneo-scleral rims (Fig. 1A) after corneal transplantation. Cells took on a spindle shape appearance, characteristic of fibroblasts (Fig. 1B). Further, nearly 100% of cells (182 out of 185 counted) expressed α-smooth muscle actin (Fig. 1C–D). In all of the following experiments, cells were treated with dexamethasone (DEX; 100 nM) to induce a steroid-response and compared to controls of media (MED) and vehicle (DMSO).

Before looking for steroid-response phenotypes based on classic TM steroid-response characteristics, the ability for scleral fibroblasts to sense and respond to steroids was tested. FKBP-51 is a well known steroid-response element for many cell-types (Davies et al., 2002;

Jääskeläinen et al., 2011; Paakinaho et al., 2010; Vermeer et al., 2003). DEX-treated cells expressed FKBP51 unlike MED- and DMSO-treated conditions (Fig. 2). This indicated that steroid-response molecular pathways were at least present in scleral fibroblasts.

Cells were then grown in an incubator with the IncuCyte Live-Cell Analysis System such that images could be taken every day. Built-in software allowed for quantitative assessment of cellular proliferation. Over time, DEX-treated cells grew slower quantitatively (Fig. 3A/B) and qualitatively (Fig. 3C–E). Assessed by automated confluence assessment (Fig. 3A), this difference was first statistically significant at 60-hours (DEX 8.4% +/− 0.4% vs. MED 11% +/− 0.4% confluence, $p < 0.001$; and DEX 8.4% +/− 0.4% vs. DMSO 9.9% +/− 0.5% confluence, $p = 0.03$). At the last time-point (~160-hours), cellular proliferation in DEX-treated cells was approximately half that of MED and DMSO (DEX 17.4% +/− 1.7% vs. MED 30.7% +/− 4.4% confluence, $p < 0.01$; and DEX 17.4% +/−1.7% vs. DMSO 31.2% +/− 5.2% confluence, $p = 0.02$). Proliferation between MED- and DMSO-treated cells was not statistically significantly different ($p = 0.94$) at the final time-point. To validate this result using another method, manual counting was done on a subset of images with masked graders (Fig. 3B). The same general result was obtained although statistical significance was not achieved for DEX compared to DMSO until 80-hours ($p = 0.01$).

DEX-treated cells also qualitatively appeared larger than MED- and DMSO-treated cells (Fig. 4). This was assessed before cells reached confluence, so that individual cells could be fully visualized. Thus DEX-treated cells were analyzed at 72-hours as opposed to 48-hours for MED- and DMSO-treated cells. Quantitatively, DEX-treated (580.8 +/− 23.1 microns^2) cells measured larger compared to MED- (453.9 +/− 18.7 microns^2) and DMSO-treated (456.9 +/− 15.5 microns^2) cells (DEX vs. MED: $p < 0.001$; DEX vs. DMSO: $p < 0.001$; and MED vs. DMSO: $p = 0.9$).

To test migration, a scratch assay was performed. Wound width, relative wound density and wound confluence were determined. Qualitatively, the DEX-treated wound appeared less confluent compared to the MED- and DMSO- treated wounds, which showed higher confluence (Fig. 5). Quantitatively, DEX-treated (1507.86 +/− 164.1 microns) cells showed a constant wound width measurement at 60 hours compared to the smaller wound width measurement in MED- (348.37 +/− 228.2 microns) and DMSO-treated (441.95 +/− 231.4 microns) cells (DEX vs. MED: $p = 0.006$; DEX vs. DMSO: $p = 0.009$; and MED vs. DMSO: $p = 0.78$; Fig. 5A). DEX-treated cells also showed a decrease in relative wound density (DEX 64.4% +/− 7.9% vs. MED 91.7% +/− 3.0%, $p = 0.02$; DEX 64.4% +/− 7.9% vs. DMSO 90.4% +/− 5.2%, $p = 0.03$; MED 91.7% +/− 3.0% vs. DMSO 90.4% +/− 5.2%, $p = 0.84$; Fig. 5B) and wound confluence (DEX 18.8% +/− 4.7% vs. MED 56.4% +/− 9.3%, $p = 0.01$; DEX 18.8% +/− 4.7% vs. DMSO 52.5% +/− 6.3%, $p = 0.005$; MED 56.4% +/− 9.3% vs. DMSO 52.5% +/− 6.3%, $p = 0.74$; Fig. 5C). Wound width, relative wound density, and wound confluence between MED- and DMSO-treated cells were not statistically significantly different.

Since steroid-response is known to alter TM cytoskeleton, Alexa Fluor-548 phalloidin (a molecule known to bind filamentous actin) labeling was performed on scleral cells. Qualitatively, in all conditions, stress fibers were seen although in DEX-treated cells the

stress fibers were more diffusely distributed (Fig. 6A/D). This was unlike MED- and DMSO-treated cells that contained stress fibers, but also had intervening regions of fewer stress fibers (Fig. 6B/E and C/F). To quantify this observation, a bin-based pixel intensity approach was taken. The average pixels per cell with a signal intensity of 0–63, 64–127, 128–191, and 192–255 were quantified. Consistent with qualitative results, DEX-treated cells had a greater number of pixels at the highest intensity range (192–255) ($p < 0.001$ to 0.004) and lesser number of pixels at the lowest intensity range (0–63) compared to controls ($p = 0.001$ to 0.008) (Fig. 6G). These results were different from that of TM cells where cross-linked actin networks (CLANs) form in response to steroids. In scleral cells, while CLANs were seen in baseline and control conditions, steroids did not increase their presence ($p = 0.73$ to 0.88) (Fig. 6H).

Since, TM cells are also known to steroid-respond by increasing expression of fibronectin and myocilin, these endpoints were tested in scleral fibroblasts as well. In both cases, after steroid exposure for 7 days, while the proteins were expressed, there was no difference comparing DEX- to MED- or DMSO-treated cells (for fibronectin $p = 0.83$ to 0.96 [Fig. 7A/B]; for myocilin $p = 0.48$ to 0.7 [Fig. 7C/D]). To test for contractility, phospho-myosin light chain was assessed. In all conditions, phospho-myosin light chain was minimally observed, but myosin light chain protein was expressed and seen by Western blot (Fig. 7E/F). Since phosphorylation events can be fleeting and steroid-response is a chronic phenomenon, we alternatively tested for contractility by looking at α-smooth muscle actin (Fig. 7 G/H). After 7-day steroid treatment, there was no α-smooth muscle actin difference comparing DEX-treated to MED- or DMSO-treated cells ($p = 0.33$ to 0.76).

Given the observation of slower growing and larger cells, it was considered that these cells may be undergoing senescence. While senescence has not been tested in TM steroid-response, TGF-β has been implicated in ocular hypertension, and TGF-β treated TM cells have been shown to undergo senescence (Yu et al., 2010). We tested this in scleral cells using a β-galactosidase senescence assay showing increased senescence in DEX-treated cells compared to controls (Fig. 8; DEX = 36.6% +/− 3.2%; MED = 21.4% +/− 3.1%; and DMSO = 20.7% +/− 1.8%) (DEX vs. MED: $p = 0.02$; DEX vs. DMSO: $p = 0.01$; MED vs. DMSO: $p = 0.97$).

4. Discussion

Steroid-response phenotypes in scleral fibroblasts were similar, but not identical, to steroid-response in TM cells. Like TM cells, steroid exposure led to larger scleral cells that proliferated and migrated less. Similar to TM cells, scleral fibroblasts also showed altered cytoskeleton; however, the morphologic appearance was different. In scleral cells, stress fibers were more distributed as opposed to showing an increased number of CLANs. Moreover, unlike TM cells, scleral fibroblasts did not increase expression of myocilin, fibronectin, or contractile properties. However, steroid-mediated gene expression pathways were intact as assessed by FKBP-51. Therefore, scleral fibroblasts are steroid responsive and share some, but not all, of the steroid-response characteristics of TM cells.

While TM cell steroid-response alterations have been studied, the exact mechanism by how these changes increase AHO outflow resistance is still unclear. Based on increased cell size and CLAN formation, it is possible that the TM becomes less porous and more stiff (Palko et al., 2016). Such a mechanism would link cellular alterations to diminished AHO. Alternatively, greater extracellular matrix deposition could be the culprit in the TM. For scleral cells, only some of the classic TM steroid-response alterations are seen. First, given that scleral cells are different from TM cells, it is not surprising that a different cell yields a similar (but slightly different) response to the same agent. However, future experiments will need to better clarify how scleral changes can impact outflow. Like for the TM (Li et al., 2019), stiffness can be measured after steroid-response, and increased stiffness has been seen in glaucomatous sclera (Palko et al., 2016). Alternatively, scleral cells may be interacting with the cells lining the outflow pathways, or the steroids may be directly impacting these cells themselves.

The exact steroid-induced molecular mechanism for scleral changes also needs further investigation. In our study, given decreased proliferation and increased cell-size we evaluated the possibility of steroid-induced senescence. This has been described for neural crest cells (Bose et al., 2010), and both TM cells and sclera have a neural crest embryologic origin (Sakao-Suzuki et al., 2014; Tripathi and Tripathi, 1989; Williams and Bohnsack, 2015). In this study, scleral fibroblast steroid exposure did induce greater senescence compared to controls (Fig. 8). While TM senescence has not been studied in relation to TM steroid-response, TM senescence is currently being actively investigated as one hypothesis for elevated IOP in glaucoma (Caprioli, 2013; Chhunchha et al., 2017; Liton et al., 2005; Yu et al., 2010). TGF-β has been implicated in glaucomatous ocular hypertension and is also noted to induce senescence in TM cells (Yu et al., 2010). As steroid-response is effectively a pharmacologically induced model for decreased outflow facility and elevated IOP in glaucoma (Li et al., 2019), senescence should also be studied in TM steroid-responsiveness in the future.

Limitations in this work include the use of scleral cells to assess distal AHO pathway steroid-response. As mentioned in the introduction and earlier in the discussion, it is more ideal to isolate and study the cells lining the outflow pathways themselves to evaluate distal (post-TM) steroid-response. This includes cells lining SC, CCs, intrascleral venous plexus, and aqueous/episcleral veins. Unfortunately, well-established and validated methods are not available for the isolation and study of these various cell types. Further, the characteristics of AHO-pathway cells that line the distal AHO pathways differ depending on where along the distal AHO pathways the cells reside. For example, cells lining CC’s may differ from cells lining episcleral veins. Episcleral veins are vascular pathways that express hallmark phylogenetic venous proteins (Gonzalez et al., 2017). SC has a hybrid origin expressing both vascular and lymphatic markers (Jung et al., 2017). Therefore, it is also unclear where along the distal pathway steroid-response is most prominent. Ongoing efforts are underway to culture the vascular distal outflow pathway cells (personal communication: Uttio Roy-Chowdhury), and steroid- responsiveness of these cells should be tested when they become available.

If it becomes difficult to isolate and validate these cells, anterior-segment perfusion cultures (Mao et al., 2011), where the distal AHO pathways are still intact, are another good model to study distal steroid-response. Recently, trabeculotomized human anterior segments have been used to study the impact of agents such as endothelin-1 and nitric-oxide donors on outflow (McDonnell et al., 2018). Since the TM was removed, any changes to the outflow facility was specifically due to direct drug impact on the distal AHO pathways themselves. These organ cultures can also last a significant period of time, up to many days (Johnson and Tschumper, 1989). Thus, the impact of steroid-response on AHO resistance can be directly studied in this model without requiring the need to specifically isolate and culture distal AHO pathway cells.

In conclusion, steroid-responsiveness is not unique to TM cells and persists distally in scleral fibroblasts. The role of steroids in medical management is complex as steroids can be both beneficial and deleterious. Steroids can slow wound-healing (both good and bad) and lead to problems such as a steroid-response IOP elevation. However, post-operatively, they are still necessary to control sequelae from overaggressive inflammation. For trabecular MIGS, the next step needs to involve innovations that improve consistency and magnitude of IOP reduction. One such step would be to better characterize post-TM MIGS steroid-response beyond clinical trial observations. Since steroid prescription can be easily titrated by a faster or slower post-operative taper or by choosing steroids with more or less ocular penetration (Pleyer et al., 2013), a better understanding of how steroids impact distal AHO pathways can lead to less steroid-response IOP elevation and better post-operative care of patients undergoing TM-targeted MIGS.

Acknowledgements

Funding for this work came from National Institutes of Health, Bethesda, MD (Grant Numbers K08EY024674 [ASH]; Research to Prevent Blindness Career Development Award 2016 [ASH]; and unrestricted grants from Research to Prevent Blindness [UCLA and UCSD] (New York, NY). The funders had no role in study design, data collection and analysis, decision to publish, or preparation of the manuscript.

References

Acott TS, Kingsley PD, Samples JR, Van Buskirk EM, 1988 Human trabecular meshwork organ culture: morphology and glycosaminoglycan synthesis. Invest Ophthalmol Vis Sci 29, 90–100. [PubMed: 3335436]

Armaly MF, 1963 Effect of Corticosteroids on Intraocular Pressure and Fluid Dynamics. I. The Effect of Dexamethasone in the Normal Eye. Arch Ophthalmol 70, 482–491. [PubMed: 14078870]

Armaly MF, 1965 Statistical Attributes of the Steroid Hypertensive Response in the Clinically Normal Eye. I. The Demonstration of Three Levels of Response. Invest Ophthalmol 4, 187–197. [PubMed: 14283012]

Becker B, 1965 Intraocular Pressure Response to Topical Corticosteroids. Invest Ophthalmol 4, 198–205. [PubMed: 14283013]

Becker B, Mills DW, 1963 Corticosteroids and Intraocular Pressure. Arch Ophthalmol 70, 500–507. [PubMed: 14078872]

Belovay GW, Naqi A, Chan BJ, Rateb M, Ahmed II, 2012 Using multiple trabecular micro-bypass stents in cataract patients to treat open-angle glaucoma. J Cataract Refract Surg 38, 1911–1917. [PubMed: 22980724]

Bill A, 1975 Editorial: The drainage of aqueous humor. Invest Ophthalmol 14, 1–3. [PubMed: 1110131]

Bose R, Moors M, Tofighi R, Cascante A, Hermanson O, Ceccatelli S, 2010 Glucocorticoids induce long-lasting effects in neural stem cells resulting in senescence-related alterations. Cell Death Dis 1, e92. [PubMed: 21368868]

Caprioli J, 2013 Glaucoma: a disease of early cellular senescence. Invest Ophthalmol Vis Sci 54, ORSF60–67. [PubMed: 24335071]

Chhunchha B, Singh P, Stamer WD, Singh DP, 2017 Prdx6 retards senescence and restores trabecular meshwork cell health by regulating reactive oxygen species. Cell Death Discov 3, 17060. [PubMed: 28904819]

Chou J, Turalba A, Hoguet A, 2017 Surgical Innovations in Glaucoma: The Transition From Trabeculectomy to MIGS. Int Ophthalmol Clin 57, 39–55. [PubMed: 28885246]

Clark AF, Brotchie D, Read AT, Hellberg P, English-Wright S, Pang IH, Ethier CR, Grierson I, 2005 Dexamethasone alters F-actin architecture and promotes cross-linked actin network formation in human trabecular meshwork tissue. Cell Motil Cytoskeleton 60, 83–95. [PubMed: 15593281]

Clark AF, Lane D, Wilson K, Miggans ST, McCartney MD, 1996 Inhibition of dexamethasone-induced cytoskeletal changes in cultured human trabecular meshwork cells by tetrahydrocortisol. Invest Ophthalmol Vis Sci 37, 805–813. [PubMed: 8603865]

Clark AF, Wilson K, McCartney MD, Miggans ST, Kunkle M, Howe W, 1994 Glucocorticoid- induced formation of cross-linked actin networks in cultured human trabecular meshwork cells. Invest Ophthalmol Vis Sci 35, 281–294. [PubMed: 8300356]

Clark AF, Wordinger RJ, 2009 The role of steroids in outflow resistance. Exp Eye Res 88, 752–759. [PubMed: 18977348]

Davies TH, Ning YM, Sánchez ER, 2002 A new first step in activation of steroid receptors: hormone-induced switching of FKBP51 and FKBP52 immunophilins. J Biol Chem 277, 4597–4600. [PubMed: 11751894]

Faralli JA, Gagen D, Filla MS, Crotti TN, Peters DM, 2013 Dexamethasone increases alphavbeta3 integrin expression and affinity through a calcineurin/NFAT pathway. Biochim Biophys Acta 1833, 3306–3313. [PubMed: 24100160]

Fellman RL, 2015 Steroids for Glaucoma: Both Friend and Foe. Review of Ophthalmology, 63–69.

Filla MS, Schwinn MK, Nosie AK, Clark RW, Peters DM, 2011 Dexamethasone-associated cross-linked actin network formation in human trabecular meshwork cells involves P3 integrin signaling. Invest Ophthalmol Vis Sci 52, 2952–2959. [PubMed: 21273548]

Filla MS, Schwinn MK, Sheibani N, Kaufman PL, Peters DM, 2009 Regulation of cross-linked actin network (CLAN) formation in human trabecular meshwork (HTM) cells by convergence of distinct beta1 and beta3 integrin pathways. Invest Ophthalmol Vis Sci 50, 5723–5731. [PubMed: 19643963]

Gonzalez JM, Ko MK, Hong YK, Weigert R, Tan JCH, 2017 Deep tissue analysis of distal aqueous drainage structures and contractile features. Sci Rep 7, 17071. [PubMed: 29213129]

Gordon DM, McLean JM, Koteen H, Bousquet FP, McCusker WD, Baras I, Wetzig P, Norton EW, 1951 The use of ACTH and cortisone in ophthalmology. Am J Ophthalmol 34, 1675–1686. [PubMed: 14894574]

Harvey BJ, Khaimi MA, 2011 A review of canaloplasty. Saudi J Ophthalmol 25, 329–336. [PubMed: 23960946]

Hernandez MR, Weinstein BI, Schwartz J, Ritch R, Gordon GG, Southren AL, 1987 Human trabecular meshwork cells in culture: morphology and extracellular matrix components. Invest Ophthalmol Vis Sci 28, 1655–1660. [PubMed: 3654139]

Huang AS, Belghith A, Dastiridou A, Chopra V, Zangwill LM, Weinreb RN, 2017a Automated circumferential construction of first-order aqueous humor outflow pathways using spectral-domain optical coherence tomography. J Biomed Opt 22, 66010. [PubMed: 28617922]

Huang AS, Camp A, Xu BY, Penteado RC, Weinreb RN, 2017b Aqueous Angiography: Aqueous Humor Outflow Imaging in Live Human Subjects. Ophthalmology 124, 1249–1251. [PubMed: 28461013]

Huang AS, Francis BA, Weinreb RN, 2018a Structural and functional imaging of aqueous humour outflow: a review. Clin Exp Ophthalmol 46, 158–168. [PubMed: 28898516]

Huang AS, Li M, Yang D, Wang H, Wang N, Weinreb RN, 2017c Aqueous Angiography in Living Nonhuman Primates Shows Segmental, Pulsatile, and Dynamic Angiographic Aqueous Humor Outflow. Ophthalmology 124, 793–803. [PubMed: 28237425]

Huang AS, Mohindroo C, Weinreb RN, 2016a Aqueous Humor Outflow Structure and Function Imaging At the Bench and Bedside: A Review. J Clin Exp Ophthalmol 7.

Huang AS, Penteado RC, Papoyan V, Voskanyan L, Weinreb RN, 2019 Aqueous Angiographic Outflow Improvement after Trabecular Microbypass in Glaucoma Patients. Ophthalmology Glaucoma 1, 11–21.

Huang AS, Penteado RC, Saha SK, Do JL, Ngai P, Hu Z, Weinreb RN, 2018b Fluorescein Aqueous Angiography in Live Normal Human Eyes. J Glaucoma 27, 957–964. [PubMed: 30095604]

Huang AS, Saraswathy S, Dastiridou A, Begian A, Legaspi H, Mohindroo C, Tan JC, Francis BA, Caprioli J, Hinton DR, Weinreb RN, 2016b Aqueous Angiography with Fluorescein and Indocyanine Green in Bovine Eyes. Transl Vis Sci Technol 5, 5.

Huang AS, Saraswathy S, Dastiridou A, Begian A, Mohindroo C, Tan JC, Francis BA, Hinton DR, Weinreb RN, 2016c Aqueous Angiography-Mediated Guidance of Trabecular Bypass Improves Angiographic Outflow in Human Enucleated Eyes. Invest Ophthalmol Vis Sci 57, 4558–4565. [PubMed: 27588614]

Jääskeläinen T, Makkonen H, Palvimo JJ, 2011 Steroid up-regulation of FKBP51 and its role in hormone signaling. Curr Opin Pharmacol 11, 326–331. [PubMed: 21531172]

Jobling AI, Nguyen M, Gentle A, McBrien NA, 2004 Isoform-specific changes in scleral transforming growth factor-beta expression and the regulation of collagen synthesis during myopia progression. J Biol Chem 279, 18121–18126. [PubMed: 14752095]

Johnson DH, Tschumper RC, 1989 The effect of organ culture on human trabecular meshwork. Exp Eye Res 49, 113–127. [PubMed: 2759186]

Johnson M, 2006 ‘What controls aqueous humour outflow resistance?’. Exp Eye Res 82, 545–557. [PubMed: 16386733]

Jung E, Gardner D, Choi D, Park E, Jin Seong Y, Yang S, Castorena-Gonzalez J, Louveau A, Zhou Z, Lee GK, Perrault DP, Lee S, Johnson M, Daghlian G, Lee M, Jin Hong Y, Kato Y, Kipnis J, Davis MJ, Wong AK, Hong YK, 2017 Development and Characterization of A Novel Prox1-EGFP Lymphatic and Schlemm’s Canal Reporter Rat. Sci Rep 7, 5577. [PubMed: 28717161]

Karmel M, 2014 Two approaches to MIGS iStent and Trabectome, EyeNet Magazine. Fajardo Dale E., San Francisco, CA, pp. 36–41.

Le K, Saheb H, 2014 iStent trabecular micro-bypass stent for open-angle glaucoma. Clin Ophthalmol 8, 1937–1945. [PubMed: 25284980]

Li G, Lee C, Agrahari V, Wang K, Navarro I, Sherwood JM, Crews K, Farsiu S, Gonzalez P, Lin CW, Mitra AK, Ethier CR, Stamer WD, 2019 In vivo measurement of trabecular meshwork stiffness in a corticosteroid-induced ocular hypertensive mouse model. Proc Natl Acad Sci U S A 116, 1714–1722. [PubMed: 30651311]

Liton PB, Challa P, Stinnett S, Luna C, Epstein DL, Gonzalez P, 2005 Cellular senescence in the glaucomatous outflow pathway. Exp Gerontol 40, 745–748. [PubMed: 16051457]

Liu J, Jung J, Francis BA, 2009 Ab interno trabeculotomy: Trabectome surgical treatment for open-angle glaucoma. Expert Reviews of Ophthalmology 4, 119–128.

Mao W, Tovar-Vidales T, Yorio T, Wordinger RJ, Clark AF, 2011 Perfusion-cultured bovine anterior segments as an ex vivo model for studying glucocorticoid-induced ocular hypertension and glaucoma. Invest Ophthalmol Vis Sci 52, 8068–8075. [PubMed: 21911581]

Matsumoto Y, Johnson DH, 1997 Dexamethasone decreases phagocytosis by human trabecular meshwork cells in situ. Invest Ophthalmol Vis Sci 38, 1902–1907. [PubMed: 9286282]

McDonnell F, Dismuke WM, Overby DR, Stamer WD, 2018 Pharmacological regulation of outflow resistance distal to Schlemm’s canal. Am J Physiol Cell Physiol 315, C44–C51. [PubMed: 29631366]

Paakinaho V, Makkonen H, Jaaskelainen T, Palvimo JJ, 2010 Glucocorticoid receptor activates poised FKBP51 locus through long-distance interactions. Mol Endocrinol 24, 511–525. [PubMed: 20093418]

Palko JR, Morris HJ, Pan X, Harman CD, Koehl KL, Gelatt KN, Plummer CE, Komaromy AM, Liu J, 2016 Influence of Age on Ocular Biomechanical Properties in a Canine Glaucoma Model with ADAMTS10 Mutation. PLoS One 11, e0156466. [PubMed: 27271467]

Phulke S, Kaushik S, Kaur S, Pandav SS, 2017 Steroid-induced Glaucoma: An Avoidable Irreversible Blindness. J Curr Glaucoma Pract 11, 67–72. [PubMed: 28924342]

Pleyer U, Ursell PG, Rama P, 2013 Intraocular pressure effects of common topical steroids for post-cataract inflammation: are they all the same? Ophthalmol Ther 2, 55–72. [PubMed: 25135807]

Polansky JR, Fauss DJ, Chen P, Chen H, Lutjen-Drecoll E, Johnson D, Kurtz RM, Ma ZD, Bloom E, Nguyen TD, 1997 Cellular pharmacology and molecular biology of the trabecular meshwork inducible glucocorticoid response gene product. Ophthalmologica 211, 126–139. [PubMed: 9176893]

Polansky JR, Fauss DJ, Zimmerman CC, 2000 Regulation of TIGR/MYOC gene expression in human trabecular meshwork cells. Eye (Lond) 14 (Pt 3B), 503–514. [PubMed: 11026980]

Sakao-Suzuki M, Kawasaki H, Akamatsu T, Meguro S, Miyajima H, Iwashita T, Tsutsui Y, Inoue N, Kosugi I, 2014 Aberrant fetal macrophage/microglial reactions to cytomegalovirus infection. Ann Clin Transl Neurol 1, 570–588. [PubMed: 25356429]

Saraswathy S, Tan JC, Yu F, Francis BA, Hinton DR, Weinreb RN, Huang AS, 2016 Aqueous Angiography: Real-Time and Physiologic Aqueous Humor Outflow Imaging. PLoS One 11, e0147176. [PubMed: 26807586]

Schneider CA, Rasband WS, Eliceiri KW, 2012 NIH Image to ImageJ: 25 years of image analysis. Nat Methods 9, 671–675. [PubMed: 22930834]

Tripathi BJ, Tripathi RC, 1989 Neural crest origin of human trabecular meshwork and its implications for the pathogenesis of glaucoma. Am J Ophthalmol 107, 583–590. [PubMed: 2729407]

Tripathi BJ, Tripathi RC, Swift HH, 1989 Hydrocortisone-induced DNA endoreplication in human trabecular cells in vitro. Exp Eye Res 49, 259–270. [PubMed: 2767172]

Tripathi RC, Tripathi BJ, 1982 Human trabecular endothelium, corneal endothelium, keratocytes, and scleral fibroblasts in primary cell culture. A comparative study of growth characteristics, morphology, and phagocytic activity by light and scanning electron microscopy. Exp Eye Res 35, 611–624. [PubMed: 6185354]

Vermeer H, Hendriks-Stegeman BI, van der Burg B, van Buul-Offers SC, Jansen M, 2003 Glucocorticoid-induced increase in lymphocytic FKBP51 messenger ribonucleic acid expression: a potential marker for glucocorticoid sensitivity, potency, and bioavailability. J Clin Endocrinol Metab 88, 277–284. [PubMed: 12519866]

Vranka JA, Acott TS, 2017 Pressure-induced expression changes in segmental flow regions of the human trabecular meshwork. Exp Eye Res 158, 67–72. [PubMed: 27334250]

Vranka JA, Bradley JM, Yang YF, Keller KE, Acott TS, 2015 Mapping molecular differences and extracellular matrix gene expression in segmental outflow pathways of the human ocular trabecular meshwork. PLoS One 10, e0122483. [PubMed: 25826404]

Weinreb RN, Polansky JR, Kramer SG, Baxter JD, 1985 Acute effects of dexamethasone on intraocular pressure in glaucoma. Invest Ophthalmol Vis Sci 26, 170–175. [PubMed: 4038695]

Williams AL, Bohnsack BL, 2015 Neural crest derivatives in ocular development: discerning the eye of the storm. Birth Defects Res C Embryo Today 105, 87–95. [PubMed: 26043871]

Wilson K, McCartney MD, Miggans ST, Clark AF, 1993 Dexamethasone induced ultrastructural changes in cultured human trabecular meshwork cells. Curr Eye Res 12, 783–793. [PubMed: 8261790]

Xie X, Akiyama G, Bogarin T, Saraswathy S, Huang AS, 2019 Visual Assessment of Aqueous Humor Outflow. Asia Pac J Ophthalmology (Phila) 8, 126–134.

Yu AL, Birke K, Moriniere J, Welge-Lussen U, 2010 TGF-{beta}2 induces senescence-associated changes in human trabecular meshwork cells. Invest Ophthalmol Vis Sci 51, 5718–5723. [PubMed: 20554622]

Highlights

- Distal steroid-response may lead to an increase in intraocular pressure (IOP)
- Increase in IOP has been observed after trabecular bypass surgery
- Scleral fibroblasts steroid-respond similar to trabecular meshwork cells
- Steroid-response in AHO pathways may contribute to IOP elevation after MIGS

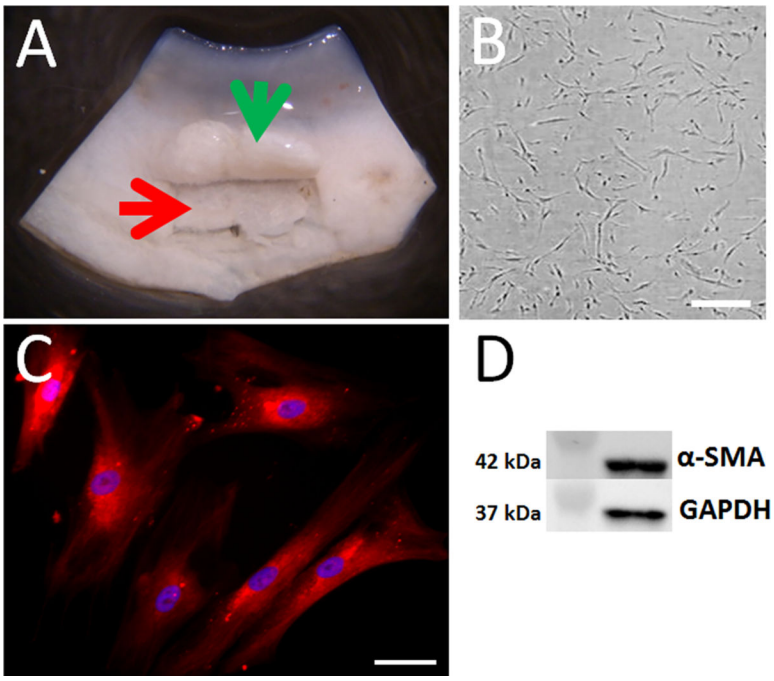

Figure 1. Primary Scleral Fibroblast Culture.

A) Cell culture was created using donor remnant corneo-scleral rims after corneal transplantation. Wedges were cut, and an initial scleral flap was made (green arrow) with a mid-depth scleral secondary flap (red arrow) created and removed for explant. B) Primary scleral cells took on a characteristic spindle shape appearance. Scale bar = 300 microns. C) Immunofluorescence confirms α-smooth muscle actin expression in nearly all primary scleral cells. Scale bar = 50 microns. D) α-smooth muscle actin protein expression was observed by Western blot. GAPDH was used as a loading control.

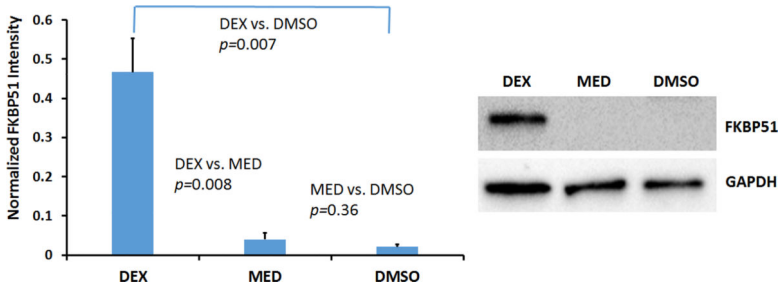

Figure 2. Primary Scleral Fibroblasts Respond to Steroid Treatment.

Elevated FKBP-51 protein expression is normally seen in response to steroid treatment. In primary scleral fibroblasts, DEX- but not MED- and DMSO-treatment induced FKBP-51 expression quantitatively and qualitatively by Western blot. GAPDH served as a loading control. Bars expressed as mean +/− SEM.

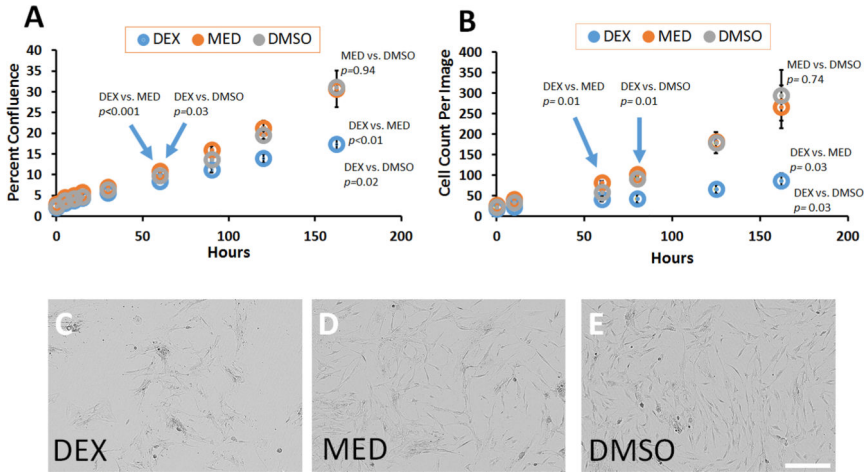

Figure 3. DEX-treatment Reduced Cellular Proliferation.

A) After DEX-treatment there was statistically significant slower cellular proliferation of primary scleral fibroblasts as assessed by automated assessment of confluence, starting at 60-hours. B) Manual counting of cells from a subset of images showed the same results with slow proliferation comparing DEX- to MED- starting at 60-hours and DEX- to DMSO- at 80 hours. Final comparisons were made at 162-hours. Data expressed as mean +/− SEM. C-E) DEX-treated cells were qualitatively less confluent at 162-hours compared to MED- and DMSO-treated cells. Scale bar = 300 microns.

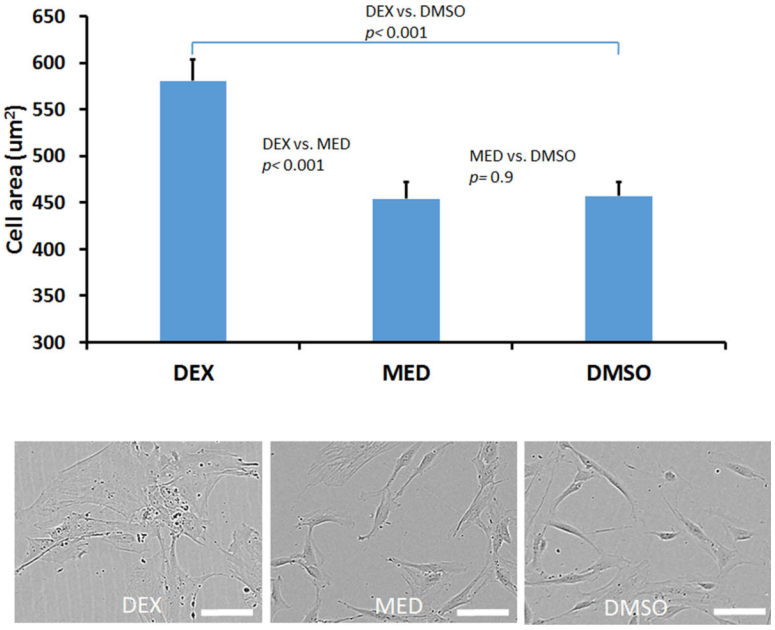

Figure 4. EX-treatment Resulted in Larger Cells.

DEX-treated cell area was quantitatively and qualitatively larger compared to MED- and DMSO-treated cells. Scale bar = 100 microns. Bars expressed as mean +/− SEM.

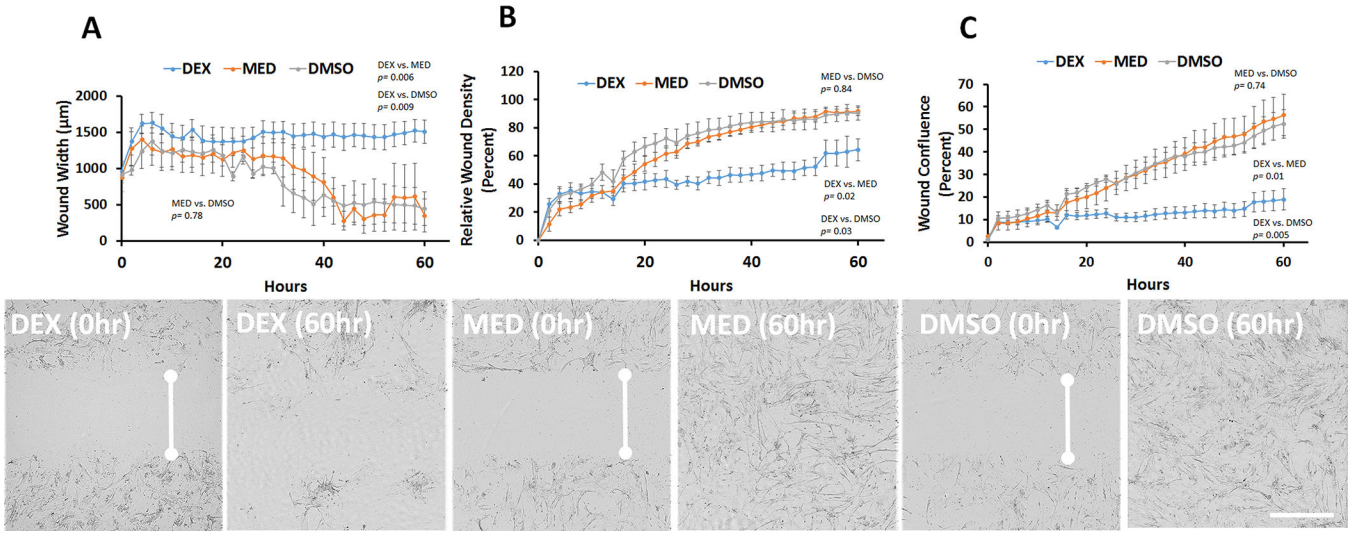

Figure 5: DEX-treatment Slowed Cellular Migration.

A-C) DEX-treated wound width analyses showed less migratory behavior compared to MED- and DMSO-treated cells. Wound width, relative wound density and wound confluence were determined by built-in IncuCyte software. Data expressed as mean +/− SEM. Qualitatively, a wound is created (0 hr; white line with round ends) in each condition from which cellular migration is assessed. At 60 hr, DEX-treated cells filled in the gap less compared to MED- and DMSO-treated cells. Scale bar = 400 microns.

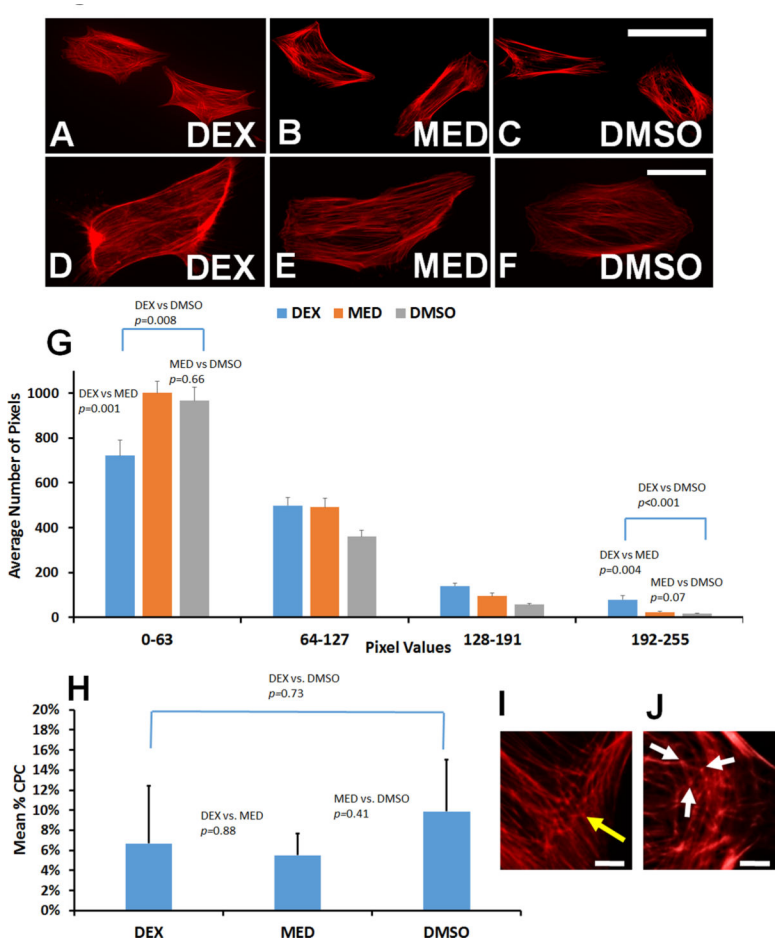

Figure 6. DEX-treatment Altered Actin Cytoskeleton.

A/D) DEX-treated cells qualitatively showed more diffuse stress fiber distribution compared to (B/E) MED- and (C/F) DMSO-treated cells. A-C) Scale bar = 100 microns. D-F) Scale bar = 50 microns. G) Quantitatively, a bin-based pixel intensity method showed that DEX-treated cells contained brighter pixels (192–255) and fewer darker pixels (0–63). H) DEX-treatment did not lead to more CLAN formation. I/J Show representative examples of CLANs at high-magnification showing a geodesic shape (yellow arrow) and an example of the minimum requirement of three intensely fluorescent vertices connected by three actin spokes (white arrows) (scale bar = 25 microns). CPC = Clan-positive cells. Bars are expressed as mean +/− SEM.

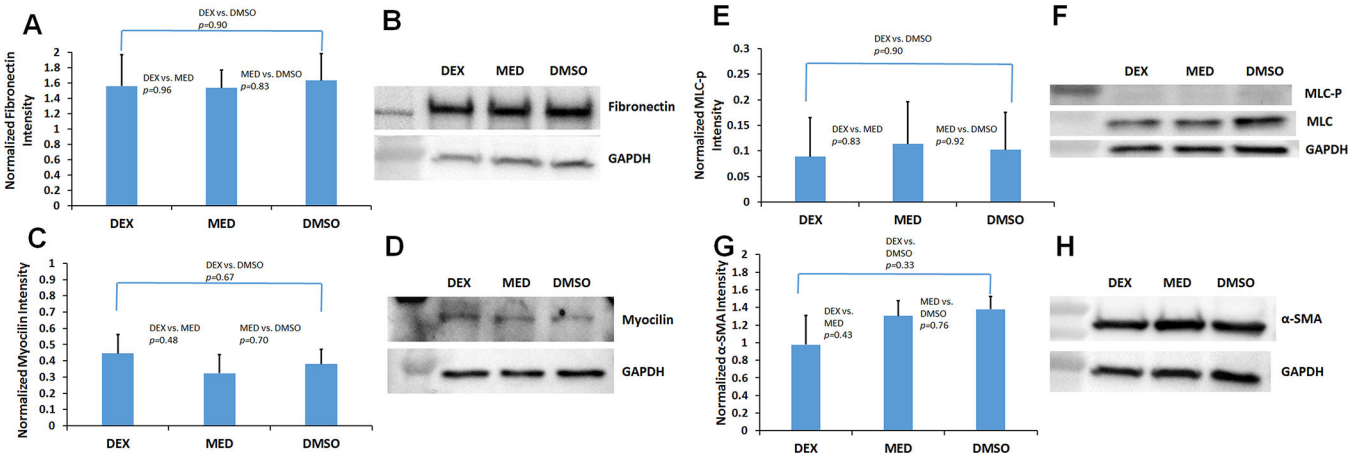

Figure 7. DEX-treatment Did Not Alter Markers of Contractility or Myocilin/Fibronectin Protein Expression.

A/B) Fibronectin was expressed in scleral fibroblasts but after 7-day DEX-treatment there was no increased protein expression compared to MED- and DMSO-treatment (n = 3 lines from 2 donors). C/D) Myocilin was expressed in scleral fibroblasts but after 7-day DEX-treatment there was no increased protein expression compared to MED- and DMSO-treatment (n = 3 lines from 2 donors). E/F) Phospho-myosin light chain (MLC-p) expression was minimal between all 3 treatment conditions (n = 3 lines from 2 donors) after 2 to 7 day DEX-treatments. Myosin-light chain (MLC) protein itself was seen though. G/H) α-smooth muscle actin was expressed in scleral fibroblasts but after 7-day DEX-treatment there was no increased protein expression compared to MED- and DMSO-treatment (n = 6 lines from 5 donors). All bars expressed as mean +/− SEM.

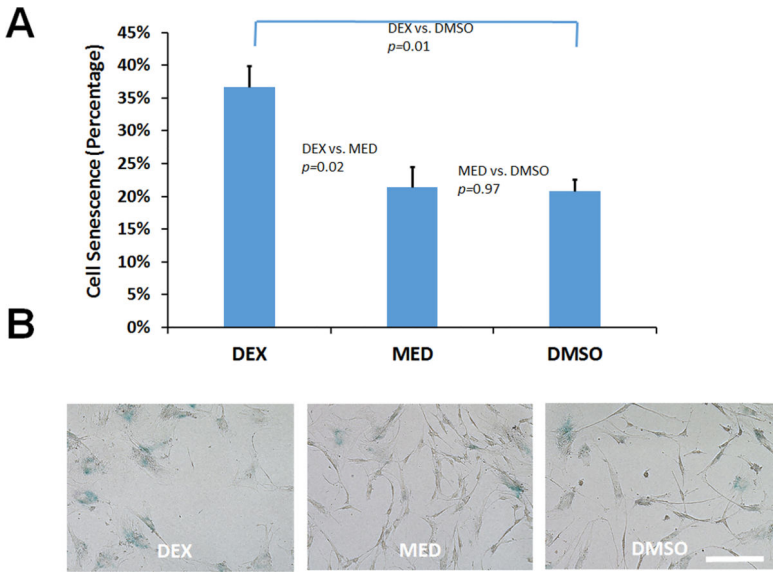

Figure 8. DEX-treatment Induces Cellular Senescence.

DEX-treated cells (A) quantitatively and (B) qualitatively (blue coloration) showed increased senescence compared to MED- and DMSO-treated cells. Scale bar = 200 microns. Bars expressed as mean +/−SEM.